RSC Advances

ROYAL SOCIETY OF CHEMISTRY

www.rsc.org/advances

Revised Manuscript *RA-ART-12-2015-026189-R-1*

Catalytic Activation and Application of Micro-spherical carbon derived from Hydrothermal Carbonization of Lignocellulosic Biomass: Statistical Analysis using Box-Behnken Design

Chowdhury Z. Z. *[1,], Abd Hamid[1†] S. B. , Rahman Md. M. [1+] and Rafique R. F. [2†]

Received: 09/12/2015; Accepted: date; Published: date

[1] Nanotechnology and Catalysis Research Center (NANOCAT),
[2] Kumoh National Institute of Technology (KIT), Gumi, South Korea,
* Correspondence: dr.zaira.chowdhury@um.edu.my; zaira.chowdhury76@gmail.com; Tel.: +603-79676959, +60102675621
† These authors contributed equally to this work.

Abstract: In this research, activated carbon was produced by physio-chemical activation of hydrothermally carbonized (HTC) derived from dried stem of *Corchorus olitorius* commonly known as Jute (JS), using potassium hydroxide (KOH) as an activation agent. The activation process was optimized using Box-Behnken Factorial Design (BBD), with outcome of 29 different experiments under predefined conditions. Four different parameters; namely activation temperature (x_1), activation time (x_2), ratio of char with KOH(x_3) and CO_2 flow rate (x_4) were optimized with respect to their influence on maximum removal percentage for divalent cations of Cu (II) (Y_1) and carbon yield (Y_2). All the four process parameters had strong positive effect on adsorption capacity up to a certain limit; beyond which it started to decline. The specific surface area of the hydrochar (HTC) was enhanced substantially after the activation process. Scanning electron microscopy (SEM) revealed that the morphology of the JS based hydrochar (JSC) changed significantly after KOH impregnation and activation under the flow of CO_2 gas. Langmuir maximum monolayer adsorption capacity for Cu (II) cations was 31.44 mg/g. Equilibrium isotherm data were well followed by Freundlich and Temkin model. Due to increase in temperature, Langmuir maximum monolayer adsorption capacity, q_m (mg/g) and Freundlich constant, K_F increased successively representing endothermic nature of adsorption.

Keywords: Hydrothermal carbonization (HTC); Langmuir monolayer adsorption capacity; Box- Behnken Design (BBD); Hydrochar; Isotherm Model, Thermodynamics

1. Introduction

The imminent shortage of non-renewable fossil fuels has commenced the search for waste lignocellulosic biomass to yield bio-carbon for waste water treatment. As the utmost profuse component in nature, lignocellulosic biomass is regarded as almost infinite bio-resources which have been used for thousands of years to produce structured as well as surface functionalized carbon materials for versatile applications [1, 2]. Thus extensive attention has been given for synthesizing biochar and hydrochar from conventional pyrolysis and hydrothermal carbonization (HTC) process [3 -7]. HTC is comparatively a

modern carbonization process where thermochemical conversion of biomass is performed at comparatively low temperatures (150– 350 ^{0}C) under autogenously created pressures. The HTC process takes place through a series of hydrolysis, condensation, decarboxylation, and dehydration reactions using deionized water as "green" solvent or acid/base or metallic ion as catalyst [8-9]. Application of HTC process is very common owing to its simplicity in design, less expenses, and energy efficiencies. Additionally, it can also be considered as ''green technique'' when water is used as catalytic medium for carbonization process [8]. Throughout the hydrothermal carbonization, the linkages between the carbohydrate rich fractions that is cellulose and hemicellulose with lignin are disrupted. Accordingly a complex cyclic-addition, aldol reactions as well as condensation reactions take place to produce hydrochar with relatively high carbon content. A number of lignin based oligomers with some sugars are dissolved in liquid phase which later on can be used for extraction of some value added products like bioplastics and biofuels. Since milder conditions are sufficient for initial carbonization, the process is energy efficient. Furthermore, it does not involve pre-drying of the raw biomass [10]. Overall the process is exothermic which releases ample heat to subsidize one-third of the energy required for complete carbonization process [10]. The process is environmentally benign as it is spontaneous whereby the huge proportion of carbon present in original biomass is retained after the carbonization process [1]. It does not produce toxic gases and tar like pyrolysis which needs additional separation technique [11]. HTC char has good self-binding properties which is advantageous for pelletisation [12]. Finally, the economical feasibility of HTC process compared to other carbonization process is that, it can be conducted without any gas flow [12].

Previous literature stated that, hydrochar prepared from biomass residues have less surface area with micro-porous texture [1, 13]. The surface morphological features can be different like nano-spheres or nano-fibers based on preparation condition [13]. It becomes hydrophilic due to presence of surface functional groups. Hydrochar contains polyfuranic structures where the furan rings are inter-connected by aliphatic chain with oxygen groups. However with increasing temperature, the aromaticity increases but the aliphatic and oxygen containing groups decreases [14]. Due to existence of oxygenated linking groups inside the final carbon matrix, it contains a lot of reactive functional groups and the structure becomes more hydrophilic than the pyrolyzed one. Thus the usage of hydrochar as initial precursors to produce activated carbon can offer an expedient approach to yield porous carbonaceous materials with desired surface chemistry to adsorb cations from water. Very few reports are available to observe the activation effect of HTC materials with different activating agent and study the physiochemical characteristics of the porous activated carbon. This leads to extensive research for developing promising carbonaceous materials for treating waste effluents before discharging [15]. Presence of various metals such as manganese (Mn), mercury (Hg), lead (Pb), cadmium (Cd), arsenic (As), copper (Cu) etc. in waste water is potentially dangerous. Among these heavy metals, copper is identified as one of the most toxic metals due to its' bio-accumulating properties. Several industries such as paper and pulp, fertilizer, wood preservatives, refineries, metal cleaning and plating bath etc. are generating copper containing waste water. Excessive consumption

of copper than the necessary limit may cause severe mucosal irritation, renal and hepatic damage, capillary damage and gastrointestinal irritation. This might be the reason for probable necrotic changes in kidney and liver of the living organisms. According to World Health Organization (WHO), maximum acceptable limit for Cu (II) concentration in drinking water should be 1.5 mg/l [16]. Thus it is essential to develop suitable adsorbent materials to eliminate excess Cu (II) metals from aqueous effluents before domestic supply.

The conventional method for preparing carbonaceous adsorbent materials by keeping one factor varying while the other variables involved at an unstipulated persistent level does not illustrate the collective influence of all the variables. In that case, the optimization process of a multivariable system typically outlines single-variable at a predefined phase. This needs a large number of experiments to be performed and fails to illustrate the interaction effects between the factors. This makes the overall process time consuming to define the optimum levels. Furthermore, it is not reliable enough for economical process design. Different types of statistical design can provide mathematical models, which can elucidate the interaction effects among the variables [17]. Among these methods, response surface methodology (RSM) based on Box Behnken Design (BBD) is one of the most appropriate methods employed recently in various fields. RSM is a collection of mathematical and statistical methods which can be employed to appraise the virtual importance of numerous affecting variables even in the manifestation of complicated interactions. Taking these into account, we have explored the feasibility of using hydrochar (JSC) prepared from dried jute stalk powder (JS) to prepare activated carbon (JSCAC) for elimination of Cu(II) cations from aqueous phase. In BBD design, the experimental variables are typically varied between two levels. This approach is considered systematic and describes nonlinear dependencies for a particular variable and interactions between the variables [18]. BBD is slightly more efficient than the central composite design (CCD) but much more efficient than the three-level full factorial designs [19]. In this research, BBD design is applied to access the effect of temperature, time, KOH ratio and CO_2 gas flow rate for activation of JSC. Adsorption experiments were conducted using the resultant carbon (JSCAC). Batch equilibrium data were analyzed using Langmuir, Freundlich and Temkin Isotherm model.

2. Materials and Methods

2. 1. Materials

2.1.1. Preparation of Feedstock (JS)

The primary biomass feedstock used for these experiments was dried jute stalk (JS). As received, the JS sample was vigorously washed with hot deionized water to remove dust and dried in an oven at 80 ^{0}C for 24 hours. To promote more effective homogeneous mixing and stirring, the sample was crushed using a ball mill. The powdered sample was sieved to remove large particles, washed, dried and stored in a sealed bottle for additional processing.

2.1.2. Hydrochar (JSC) Preparation

The waste lignocellulosic residues of JS are not utilized properly; usually they are decomposed or burnt after extraction of the fiber. During preparation of hydrochar 7 g of JS

powder was mixed with 70 mL of deionized water and stirred until it was homogeneously mixed. Thus prepared sample was transferred into a Teflon-lined autoclave (100 mL). The temperature was ramped to 220 ^{0}C and carbonized for 4 h. The resulting char sample (JSC) was washed several times with de-ionized water until a neutral pH was obtained. The hydrochar (JSC) thus obtained was not initially activated and stored in air-tight vessels for preliminary characterization studies.

2.1.3. Activation of Hydrochar (JSC) to prepare Activated carbon (JSCAC)

JSC was further impregnated with predefined ratio of KOH based on basic design matrix of BBD (Table 2). During impregnation, 100 mL deionized water was mixed with the char (JSC) and KOH pellets. The resultant mixture was heated at 90–100 °C for 4 h. The sample was kept overnight in an oven at 90 °C. The dried sample was further pyrolyzed to initiate activation process to yield final product with enlarged surface area. The activation process was carried out in the presence of CO_2 gas flow at pre-defined conditions (Table 1 and Table 2). The activated carbon sample (JSCAC) thus obtained was washed vigorously in order to remove unreacted KOH attached with the surface. The carbon samples got after two stage of physiochemical activation were dried and stored for further characterization and isotherm studies.

2.2. Methods

2.2.1. Isotherm and Thermodynamic Characterization for Single Solute System

Requisite amount of $CuSO_4.5H_2O$ salt were dissolved in 1000 mL of deionized water to prepare the stock solution of Cu(II) cations having concentration of 1000 mg/L. The stock solution was further diluted to obtain test solutions having concentration of 50, 60, 70, 80, 90 and 100 mg/L for isotherm studies. For removal percentage calculation, highest solution concentration, 100 mg/L was agitated with 0.2 gm of JSCAC sample (Table 2). Adsorption experiment was carried out at (30±1) ^{0}C around 250 rpm. Prior to agitation, the solution pH was adjusted to 5.5 for isotherm characterization of the equilibrium system. The amount of Cu(II) cations adsorbed onto the surface of JSCAC was calculated by the following equation [20, 21]:

$$q_e = \frac{(C_0 - C_e)V}{W} \tag{14}$$

Here, q_e (mg/g) denotes the quantity of cation loaded at equilibrium; C_0 is the initial concentration of the targeted cation; C_e (mg/L) is the residual equilibrium concentrations of metal ions at liquid phase; V (L) represents the volume of the single solute solution; and W (g) is the mass of JSCAC used. For calculating removal percentages at different experimental condition based on Table 2, following equation was used:

$$\%\,\mathrm{Re}\,moval = \frac{(C_0 - C_e)}{C_0} x100 \tag{15}$$

2.2.2. Experimental Design

Box Behnken design (BBD) based on RSM method was used here to examine the impact of different effective factors on Cu(II) cations adsorption efficiency. Simultaneously it can determine the most appropriate permutation of variables ensuing in maximum removal efficiency with highest process yield. The Box Behnken Design (BBD) with four factors, involving five replicates at the center point for assessment of residual errors was used to

obtain the basic design matrix (Table 2). It was used to develop a second-order polynomial model with linear, interaction and quadratic terms. For the activation of JSC, four important effective parameters such as temperature (x_1), time (x_2), ratio (x_3) and CO_2 flow rate (x_4) were considered as the independent variables, while the removal efficiencies of Cu (II) (Y_1) and yield (Y_2) were the responses (dependent variable). Overall the optimization process contains three major steps of statistically designing and performing the experiments, determining the coefficients in a mathematical model and analyzing the adequacy of the model according to following equation (3) [27]:

$$Y = f(x_1, x_2, x_3, x_4 - - - - - x_n) \tag{16}$$

Where, Y is the response of the system and X_i is the variables under investigation for the process. Temperature was varied from 600 to 1000 ^{0}C, time from 1-3 h, char with KOH ratio 0.5 to 2 and CO_2 flow rate was changed from 50 to 100 mg/L. The low, middle, and high levels of each variable were indicated as -1, 0, and +1, respectively. It is essential to find a proper estimation for the precise functional relationship between the independent variables and the selected responses for optimization [21]. The number of experiments (N) required for BBD design is expressed by:

$$N = 2k(k-1) + C_0 \tag{17}$$

Where k is number of factors and Co is the number of central points. This method is less time consuming, when k is not too large [16]. The order of experimental run was randomized and the responses were used to develop empirical models that can correlate the responses of removal efficiencies with yield using a second-degree polynomial equation as given by equation (23):

$$Y = b_0 + \sum_{i=1}^{n} b_1 x_1 + \sum_{i=1}^{n} b_{11} x_i^2 + \sum_{i=1}^{n} \sum_{j>1}^{n} b_{ij} x_i x_j \tag{18}$$

Where, Y is the predicted response, b_0 the constant coefficient, b_1 the linear coefficients, b_{ij} the interaction coefficients, b_{ii} the quadratic coefficients and x_i, x_j are the coded values of the adsorption [27]. For four variables, the suggested number of experiments at the center point is five and the total number of experiments (N) required are 29 (Table 2). Table 2 summarizes the coded and actual levels of four independent variables together with the responses obtained for BBD experimental design matrix.

2.2.2. Characterization

JS, JSC and JSCAC were characterized by several analytical techniques to identify the surface properties of the prepared samples. The surface morphological changes of final products were characterized using a field emission scanning electron microscope (FE-SEM) (Zeiss SUPRA 35VP; Germany). The BET Surface area, micro pore, meso pore volume

and pore size distribution of the samples were analyzed using TriStar II BET Surface Area Analyzer. Prior to nitrogen gas adsorption, the samples were outgassed under vacuum at 300 °C for 4 h to remove moisture content. Surface area and pore diameter was calculated by Brunauer-Emmett-Teller (BET) method, whereas micropore volume was obtained by the t-plot method. The crystalline structure of the samples was analyzed using X-ray diffraction (XRD, Burker AXSD8 Avance, Germany) at 40 kV and 40 mA using Cu-Kα radiation sources. Thermogravimetric analysis coupled with a differential thermal analyzer (DTA) (Mettler Toledo Star SW901, Japan) was carried out to determine the thermal stability of the samples under a 5 mL/min nitrogen flow. In the TGA analysis, 7 mg of each sample was heated under a N_2 flow at 1000 °C with a heating rate of 5 °C/min. Ultimate analysis (Elemental Analyzer- PerkinElmer, Series II 2400) was carried out to calculate the percentage of carbon, hydrogen, and nitrogen in JS, JSC and the final carbon, JSCAC.

3. Results and Discussion

3.1. Statistical Analysis for Model Validation

The level of process variables with the design matrix with outcome of 29 numbers of experiments and the output responses are shown in Table 1 and Table 2 respectively. Five replicate runs were performed at the center point for the estimation pure error.

Table 1. Independent variables for Activation of JSC with their coded and actual level

Variables	**Code**	**Units**	**Coded and Actual Variable Levels**		
			-1	**0**	**+1**
Temperature	x_1	°C	600	800	1000
Activation Time	x_2	Hour	1	2	3
Ratio (Hydrochar: KOH)	x_3	-	0.5	1.25	2
CO_2 gas Flow Rate	x_4	mg/L	50	75	100

Table 2. Experimental Responses for Cu (II) removal percentages (Y_1) and Carbon Yield (Y_2) for JSCAC

Standard Order	Run	Type of Point	Reaction Variables (Actual Factors)				Removal %	Yield %
Order	No	Point	Temperature(x_1) (°C)	Time(x_2)(h)	Ratio (x_3)	Flow Rate (x_4) (mg/L)	Y_1	Y_2
1	1	IBFact	600	1	1.25	75	82.33	46.88
2	2	IBFact	1000	1	1.25	75	86.32	30.76
3	10	IBFact	600	3	1.25	50	83.99	39.99
4	11	IBFact	1000	3	1.25	50	84.99	26.66
5	17	IBFact	800	2	0.50	100	85.88	41.09
6	3	IBFact	800	2	2	100	91.88	40.89
7	4	IBFact	800	2	0.50	50	85.78	35.88
8	5	IBFact	800	2	2	50	86.09	31.78
9	6	IBFact	600	2	1.25	100	81.89	45.66
10	7	IBFact	1000	2	1.25	100	88.23	31.09
11	8	IBFact	600	2	1.25	75	81.66	41.89
12	9	IBFact	1000	2	1.25	75	85.03	26.76
13	12	IBFact	800	1	0.50	75	84.89	38.99
14	13	IBFact	800	3	0.50	75	86.98	36.77
15	14	IBFact	800	1	2	75	90.09	41.99
16	15	IBFact	800	3	2	75	88.78	33.98
17	16	IBFact	600	2	0.50	75	80.99	48.48
18	17	IBFact	1000	2	0.50	75	88.29	29.06
19	18	IBFact	600	2	2	50	83.46	42.89
20	19	IBFact	1000	2	2	50	87.20	28.79
21	20	IBFact	800	1	1.25	100	86.90	43.88
22	21	IBFact	800	3	1.25	100	89.88	39.89
23	22	IBFact	800	1	1.25	75	87.89	34.77
24	23	IBFact	800	3	1.25	75	81.67	32.88
25	24	Center	800	2	1.25	75	90.88	37.44
26	25	Center	800	2	1.25	75	91.09	37.48
27	27	Center	800	2	1.25	75	90.77	37.05
28	28	Center	800	2	1.25	75	91.08	37.29
29	29	Center	800	2	1.25	75	91.98	36.99

Three tests are necessary to estimate the accuracy of the prepared model for statistical analysis. In this context, three different tests explicitly sequential model sum of squares, lack of fit tests and model summary statistics were observed in this research. Cubic model was not suggested for removal percentage (Y1) and yield (Y2) due to insufficient points for calculating the coefficients for this kind of the model. Based on sequential model sum of the squares and model summary statistics, quadratic model showed the best fit with the experimental data having the lowest standard deviation, the highest correlation coefficient R2 and adjusted R2 values for Cu(II) removal percentages (Y1). 2FI model containing constant term with positive sign, variables (x_1, x_2, x_3 and x_4) and interaction terms (x_1x_2, x_2x_3, x_3x_4 *and* x_4x_1) with co-efficient was proposed by the software for yield (Y_2) calculation. The model articulated by equation (1), represents the removal percentage of Cu (II) cations by prepared carbon JSCAC (Y_1) in terms of their coded values. The final yield of the carbon sample (Y_2) is expressed by equation (2). Both the response equations were derived as a function of temperature (x_1), retention time (x_2), hydrochar with KOH ratio (x_3) and the rate CO_2 gas flow during the activation process (x_4).

$$\%Cu(II)\,\mathrm{Re}moval = +92.16 + 2.15x_1 - 0.18x_2 + 1.22x_3 - 1.38x_4 - 0.75x_1x_2 - 0.89x_1x_3 - 0.74x_1x_4 - 0.85x_2x_3 - 2.30x_2x_4 - 1.42x_3x_4 - 4.66x_1^2 - 2.12x_2^2 - 1.42x_3^2 - 2.36x_4^2 \quad (1)$$

$$\%Yield = +37.19 - 7.76x_1 - 2.26x_2 - 0.59x_3 - 3.48x_4 + 0.70x_1x_2 + 0.62x_1x_3 + 0.67x_1x_4 - 1.45x_2x_4 - 0.97x_3x_4 \quad (2)$$

The coefficients containing independent variables of temperature (x_1), time (x_2), ratio of KOH (x_3) and CO_2 flow rate (x_4) denote the influence of that specific factor on the responses of removal percentage of Cu (II) (Y_1) and yield (Y_2). Multiplication values between the two factors and others with second order terms exhibit the interaction and quadratic effect, respectively [24, 25]. A positive sign in front of the constant terms indicates a synergistic effect, whereas a negative sign indicates an antagonistic effect [26]. The high values of regression coefficient, R^2 for all the two responses (Table 3) indicated that the predicted results for model fitting were reasonably similar with the experimental observations. The R^2 value for equations (1) and equation (2) are 0.952 and 0.978 which is nearer to unity reflecting better suitability of the developed models. The values obtained for Co-efficient of Variation (CV) and standard deviations were small which shows reproducibility of the developed models. The values of adequate precision were calculated based on signal to noise ratio [24, 25]. For effective model simulation, adequate precision should be larger than 4. The adequate precision observed for percentage Cu (II) removal and yield were 14.19 and 33.77. Thus it can be concluded that the experimental data obtained here is statistically significant to navigate the design [26].

Table 3. Statistical Parameters for Model Accuracy Test

Statistical Parameters	**Removal %** Y_1	**Yield %** Y_3
Standard Deviation, SD%	1.04	1.10
Correlation Coefficient, R^2	0.952	0.978
Adjusted R^2	0.904	0.965
Mean	86.79	37.14
Coefficient of Variation, CV	1.19	2.96
Adequate Precision	14.19	33.17

Figure 1(a) and 1(b) illustrate the studentized residuals versus the actual values obtained for each experimental run for removal percentage (Y_1) and yield (Y_2) respectively. The data obtained after residual analysis are arbitrarily distributed about zero. This demonstrates that the variance of the experimental interpretations is almost constant for 29 experimental run. All of the data points observed are found to fall within the range of +3 to -3. This confirms that response transformation is not needed for the experimental design applied here [27].

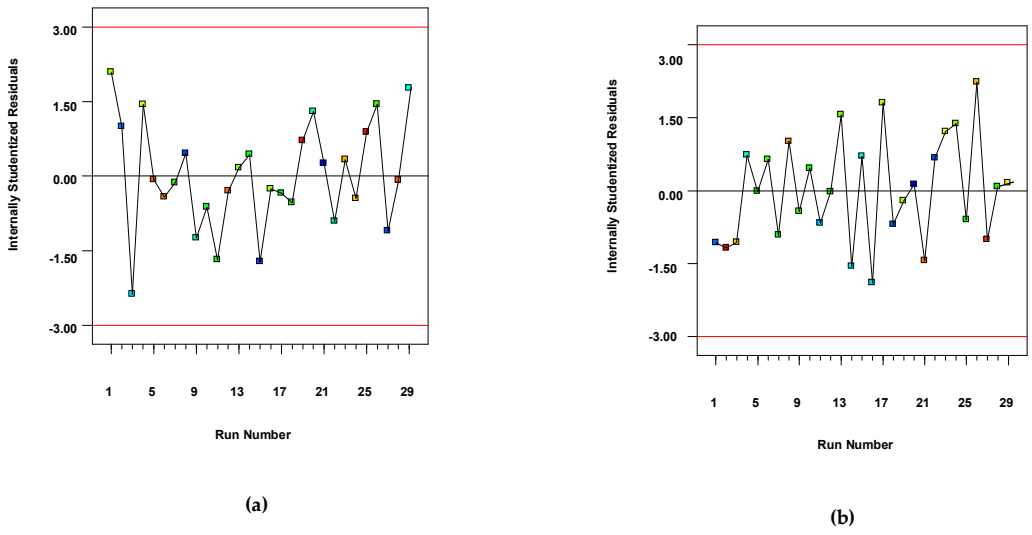

Figure 1. Studentized residuals *versus* Actual values for experimental run (a) Removal percentages, Y_1 of Cu(II) cations (b) Yield percentages (Y_2) of JSCAC

Table 4 and 5 illustrate the result of ANOVA analysis for removal percentage (Y_1) and yield (Y_2) respectively, where the F-test revealed that these regressions are statistically significant at 95% confidence level.

Table 4. Analysis of Variance (ANOVA) and Lack of Fit test for Removal % of Cu (II) cations onto JSCAC (Y_1).

Source	Sum of	Degree of	Mean	F Value	Prob> F	Comments
Model	298.91	14	21.35	19.86	<0.0001	*Significant*
x_1	55.21	1	55.21	51.36	<0.0001	
x_2	0.38	1	0.38	0.35	0.5626	
x_3	17.98	1	17.98	16.73	0.0011	
x_4	22.80	1	22.80	21.21	0.0004	
x_1^2	140.93	1	140.93	131.10	<0.0001	
x_2^2	29.15	1	29.15	27.12	0.0010	
x_3^2	13.08	1	13.08	12.17	0.0360	
x_4^2	*36.17*	1	*36.17*	33.64	0.0010	
x_1x_2	2.24	1	2.24	2.08	0.1713	
x_1x_3	3.17	1	3.17	2.95	0.1081	
x_1x_4	2.21	1	2.21	2.05	0.1740	
x_2x_3	2.89	1	2.89	2.69	0.1234	
x_2x_4	21.16	1	21.16	19.68	0.0006	
x_3x_4	8.09	1	8.09	7.53	0.0158	
Residuals	15.05	14	1.08			
Lack of Fit	14.14	10	1.41	6.19	0.0470	*Significant*
Pure Error	0.91	4	0.23			

F-test values representing the deviation in data about the mean were determined to check the competence of the models. The model F-value for removal percentage of Cu (II) cations and yield were 19.86 and 78.63 respectively which inferred that these models were significant. However, the values of Prob > F values for all these two responses were less than 0.05, which specified that the model terms considered here for response analysis were significant [23, 24]. For the response of removal percentage, Y_1, the linear factors of temperature (x_1), ratio (x_3), flow rate (x_4) as well as their quadratic terms ($x_1^2 x_3^2 x_4^2$) were significant. The interaction terms of time with flow rate (x_2x_4) and ratio with flow rate (x_3x_4) were also the significant model terms. Compared to temperature (x_1) and flow rate (x_4), other linear terms of time (x_2) and ratio (x_3) had moderate influence on removal percentage (Y_1). The interaction influence of time and CO_2 flow rate (x_2x_4) was more prominent (owing to the highest value of F) than the other interaction factors related to the percentage removal, Y_1.

Table 5. Analysis of Variance (ANOVA) and Lack of Fit test for Yield % (Y_2)

Source	Sum of Squares	Degree of Freedom	Mean Square	F Value	Prob> F	Comments
Model	951.40	10	95.19	78.63	<0.0001	*Significant*
x_1	721.99	1	721.99	596.67	<0.0001	
x_2	61.20	1	61.20	50.58	<0.0001	
x_3	4.24	1	4.24	3.50	0.0777	
x_4	145.39	1	145.39	120.16	<0.0001	
x_1x_2	1.95	1	1.95	1.16	0.2209	
x_1x_3	1.56	1	1.56	1.29	0.2707	
x_1x_4	1.78	1	1.78	1.47	0.2406	
x_2x_3	8.38	1	8.38	6.93	0.0169	
x_2x_4	1.10	1	1.10	0.91	0.3525	
x_3x_4	3.80	1	3.80	3.14	0.0932	
Residuals	21.78	18	1.21			
Lack of Fit	21.57	14	1.54	29.30	0.0025	*Significant*
Pure Error	0.21	4	0.053			

For yield percentages (Y_2), activation temperature (x_1), activation time (x_2), and CO_2 flow rate (x_4) were significant to the response. However, the interaction influence of x_2x_3 and x_3x_4 had greatest impact on yield percentages. This phenomenon can be observed from Table 2 (Run 9 and 17). Experimental run 9 and 17 were using same temperature of 600^0C with residence time of 2 hours. In run 17, comparatively lesser ratio (0.50) with flow rate (75 mg/L) were used than run 9 (Ratio 1.25, Flow rate 100). Interaction effect of ratio and flow rate (x_3x_4) was prominent to give lesser yield of 45.66% in run 9 compared to run 17 (48.89%). Like removal percentages (Y_1), temperature (x_1) had the highest impact on yield (Y_2) calculation.

3.2. Influence of Functional Variables on Cu(II) uptake

The physiochemical characteristics of an ideal activated carbon should ensure high removal efficiencies. In that case, the carbon sample (JSCAC) should have a large BET surface area with appropriate pore size distribution which can facilitate for the liquid phase adsorption process. The influence of the four variables on the removal percentage of Cu (II) cations were investigated by RSM using three-dimensional response surface with two dimensional contour plots. From the response surface analysis, it was observed that all the four variables had cumulative effect in elevating the removal efficiencies (Y_1) up to a certain level.

Figure 2 (a) shows the interactions between temperature (x_1) and time (x_2) on removal efficiencies (Y_1) when the other variables of ratio (x_3) and CO_2 flow rate (x_4) were fixed at center point (x_3= 1.25, x_4= 75 mg/L). Figure 3(b) illustrates the effect of time (x_2) and ratio (x_3) onto removal percentages (Y_1) when temperature (x_1) and CO_2 flow rate (x_4) were fixed at center point (x_1= 800 ^{0}C, x_4= 75 mg/L). The values on the X and Y-axis are the real values.

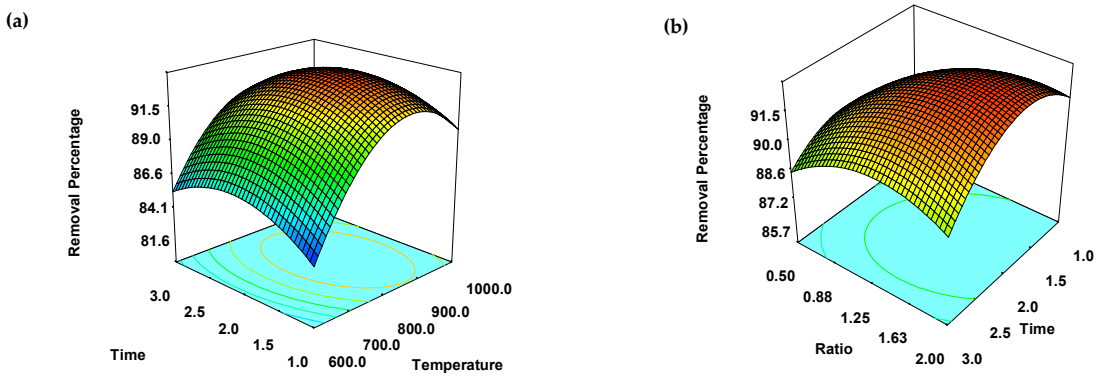

Figure 2. 3-D Response Surface Contour plots of the combined effects of (a) Temperature (x_1) and Time (x_2) (b) Time (x_2) and Ratio (x_3) on % Removal of Cu (II) cations onto JSCAC (Y_1) when the other variables are at center points

Figure 2(a) and 2(b) show that higher temperature and longer retention time enhances the removal efficiencies up to a certain level giving concave pattern of the RSM plots. The highest value of removal percentage recorded was about 91.98% (Run 6: temperature (x_1) =800 ^{0}C, time (x_2) = 2h ratio (x_3) = 1.25 and flow rate (x_4) = 75mg/L). This is because, during the activation process, the proliferation in temperature and residence time would release more volatile component as a result of intensified dehydration and elimination reactions. Longer retention time would facilitate more contact between char matrix with KOH and CO_2 gas to enhance the surface area [26, 28].

Figure 3(a) shows the interactions between temperature (x_1) and ratio (x_3) on removal efficiencies (Y_1) when the other variables of time (x_2) and CO_2 flow rate (x_4) were fixed at center point (x_2= 2h, x_4= 75 mg/L). Figure 3(b) illustrates the effect of temperature (x_1) and CO_2 flow rate (x_4) onto removal percentages (Y_1) when time (x_2) and ratio (x_3) were fixed at center point (x_2=2 h, x_3= 1.25). From the curvature of these plots, it reveals that the temperature (x_1) and ratio (x_3) of impregnating base is proportional with the removal percentages. It appears that, up to a fixed limit; the increase of temperature and ratio of activating base in presence of CO_2 gas flow will enhance the reaction rate between KOH and hydrochar resulting more porous texture which is desirable for adsorption. Thus when ration (x_3) was increased with temperature up to a certain extent removal percentage (Y_1) of Cu (II) cations was increased. After certain limit, enhancing temperature (x_1) and ratio (x_3) was unfavourable for adsorption process. This was expected as too high temperature or KOH concentration might destroy some surface functional groups. It might destroy the porous texture of prepared carbon by thermal annealing which will abolish the walls of pores reducing the pore volume [30, 31].

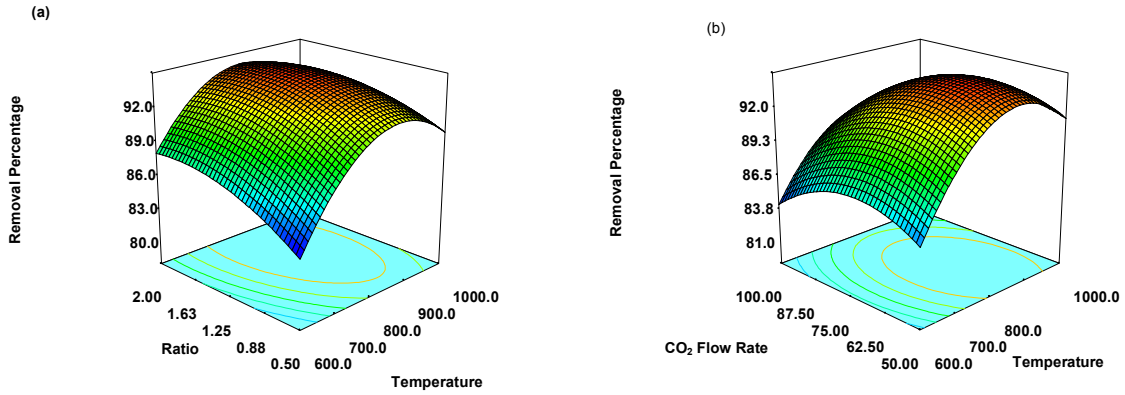

Figure 3. 3-D Response Surface Contour plots of the combined effects of (a) Temperature (x_1) and Ratio (x_3) (b) Temperature (x_1) and CO_2 Flow Rate (x_4) on % Removal of Cu(II) cations onto JSCAC (Y_1) when the other variables are at center points

Previous literature showed that, the activation time had moderate to minimum effect on enhancing the surface area and pore structure of the activated carbon prepared from cassava peel whereas the pore distribution in terms of micro and meso-pore percentages were strongly influenced by KOH impregnation ratio and temperature [28]. Too short activation time and too lower temperature might not be sufficient to enhance the surface area up to a greater extent [28]. Lower temperature will allow the volatile matters to reside inside the pores impeding the pore development. At very high temperature and longer residence time with high ratio of KOH, the carbon skeleton might burn out to produce more ash which also can contribute in lower removal efficiency. Too long contact time for activation is not suggested as it might increase the liquid yield, lessen carbon yield with successive decrease in removal efficiency. In addition to that, longer contact time also evidently means greater expenses as the high activation temperature needs be retained for a longer period of time [32]. This trend was also observed in previous literature during preparing activated carbon for removal of Zn (II) cations using oil palm fronds [33]. Progressive increase in temperature (x_1) and flow rate (x_4) facilitate the volatilization process of the low molecular weight organic substances which consequently results in higher surface area of the prepared carbon (JSCAC) [34, 35, 36]. Increment in temperature enhances the activation process which is endothermic and leads to the removal of disorganized carbon [37]. This will expose more aromatic sheets of carbon to react with CO_2 gas [36]. It was observed that, an increase in flow rate (x_4) until moderate temperature (x_1) enhances the removal efficiencies. But, at a point where the flow rate (x_4) or the retention temperature (x_1) was too high, the removal efficiencies decreased. This is due to the extreme burn-off of carbon. Thus it can be concluded that increasing temperature (x_1) and flow rate (x_4) beyond the optimum limit will destroy the pore structure resulting lower BET surface area with less removal efficiencies (Y_1). However, at very low CO_2 flow rate and reaction time, the removal percentage was lower. This happens due to insufficient contact time between KOH impregnated hydrochar

(JSC) and the CO_2 gas which adversely affects the quality of the prepared carbon (JSCAC) [38].

3.3. Influence of Functioning Variables on Yield percentages

Figure 4a reveals the cumulative influence of two independent factors temperature(x_1) and time (x_2) on percentage yield of carbon (Y_2) where KOH ratio(x_3) and CO_2 gas flow (x_4) were fixed at center point. Figure 4b showed the combined impact of time (x_2) and KOH ratio (x_3) over yield percentage (Y_2), where the temperature (x_1) and flow rate (x_4) were kept at center point.

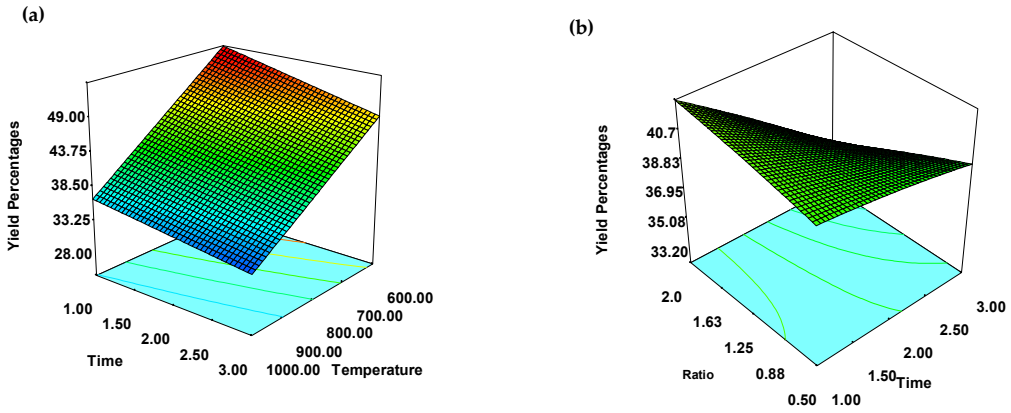

Figure 4. 3-D Response Surface Contour plots of the combined effects of (a) Temperature (x_1) and Time (x_2) (b) Time (x_2) and Ratio (x_3) on % Yield of JSCAC (Y_2) when the other variables are at center points

In this research, all the four parameters investigated had synergistic influence on percentage yield (Y_2). It was found that when the activation temperature (x_1), retention time (x_2), ratio(x_3) and flow rate of CO_2 (x_4) were increased, the yield percentage decreased significantly. Temperature (x_1) had highest impact on yield percentage (Y_2) which was earlier shown by the highest F value of 543.08, as shown by Table 5, whereas activation ratio (x_3) was less noteworthy compared to activation temperature (x_1), time (x_2) and flow rate (x_4). The lowest yield was obtained when temperature was at 1000°C for 3 h using KOH ratio 1.25 under the flow rate of 75mg/L (Run 22) as shown by Table 2. The enhancement of temperature, contact time, ratio and flow rate will intensify the diffusion of basic medium inside the hydrochar matrix leading to conversion of carbon with ash residues. This would further initiate the disintegration of the crystalline region of hydrochar and form carbon with amorphous texture which is desirable for adsorbent preparation. This observation is consistent with the previous work carried out for activation of cassava peel [28], where activation temperature was found to play a vigorous role on the carbon yield, whereas activation time showed least impact on yield.

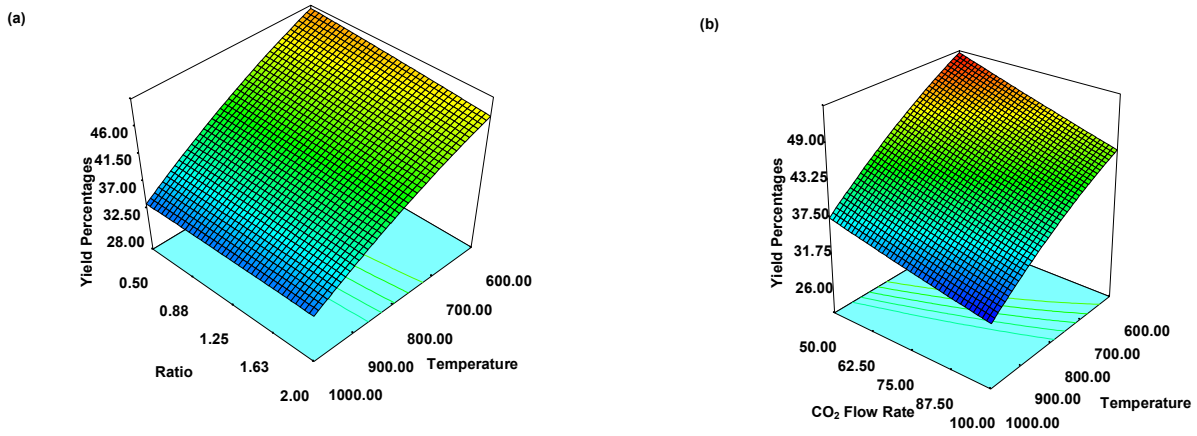

Figure 5. 3-D Response Surface Contour plots of the combined effects of (a) Temperature (x_1) and Ratio (x_3) (b) Temperature (x_1) and CO_2 Flow Rate (x_4) on % Yield of JSCAC (Y_2) when the other variables are at center points

However, using higher reaction temperature (x_1) with higher ratio (x_3) would result in lower yield percentages (Y_2) (Figure 5a). The increase in temperature and flow rate together would gradually enhance more dehydration and elimination reactions to release additional volatile organic fractions from hydrochar matrix as gas and liquid products rather than solid activated carbon (Figure 5b).

3.4. Optimizing operating conditions

For successful process design in case of adsorption process, relatively high removal efficiencies are expected for targeted pollutant under optimum condition. As observed from the basic design matrix that, when the values of process variables were increasing, percentage removal was increasing up to a certain limit whereas yield was decreasing and vice versa. The numerical optimization menu was selected using Design Expert software version 8.0.6 (STAT-EASE Inc., Minneapolis, LTS). In order to optimize the adsorption process, the targeted goal was set as maximum values for removal percentage and yield, while the values of the temperature, time, ratio and CO_2 flow rate were set in the ranges being studied as depicted earlier by previous literature [2]. The error was evaluated and provided by Table 6.

Table 6. Numerical Optimization for Process Design

Temperature	Time	Ratio	Gas Flow	Percentage Removal			Percentage Yield		
(x_1)	(x_2)	(x_3)	(x_4)	(Y_1)			(Y_2)		
(°C)	(h)	-	mg/L	Predicted	Experimental	Error	Predicted	Experimental	Error
752.93	1.86	2.00	51.23	90.55	91.75	1.30	43.02	42.87	0.348

3.5. Application of JSCAC for Liquid Phase Adsorption: Equilibrium Isotherm Studies

Isotherm parameters were determined using linear model equations, i.e. Langmuir, Freundlich, and Temkin for temperature 30, 50 and 70 ^{0}C. Maximum monolayer sorption quantity, q_m (mg/g) and Langmuir constant K_L (L/mg) demonstrating the binding energy for adsorption uptake were determined for Cu(II) adsorption onto JSCAC using Langmuir model equation 7 [39]:

$$q_e = \frac{K_L C_e}{1 + a_L C_e} \tag{7}$$

The nonlinear form of equation (7) was linearized to give equation (8):

$$\frac{C_e}{q_e} = \frac{1}{q_{max} K_L} + \frac{1}{q_{max}} C_e \tag{8}$$

The dimensionless factor, R_L, of the Langmuir model can be calculated using equation 9:

$$R_L = \frac{1}{1 + K_L C_o} \tag{9}$$

In this present research, R_L values are determined for the highest initial concentration (100 mg/L). R_L was determined to get specific idea about the types of isotherm, as illustrated by Table 10 [40].

Table 7. Isotherm Types based on Separation Factor R_L.

Value of R_L	Magnitude	Types of Isotherm
$R_L > 1$	Greater than one	Unfavorable
$R_L = 1$	Equal to one	Linear
$0 < R_L < 1$	Between zero to one	Favorable
$R_L = 0$	Zero	Irreversible

Freundlich isotherm provides insight about the surface heterogeneity. It shows the multilayer sorption characteristics of Cu(II) cations onto JSCAC . The empirical equation shows that the reactive sites over the carbon sample are scattered exponentially with the heat of the adsorption method [41]. The nonlinear form of Freundlich equation is given by:

$$q_e = K_f C_e^{1/n} \tag{10}$$

The above equation was linearized to determine the parameters and is represented by equation (11):

$$\ln q_e = \ln K_f + \frac{1}{n}\ln C_e \quad (11)$$

Here, K_f (mg/g) is the affinity factor of the cations towards the carbon sample (JSCAC) and $1/n$ represents the intensity of the adsorption.

Equilibrium data was further analyzed by the Temkin isotherm and are expressed by [42]:

$$q_e = \frac{RT}{b}\ln K_T C_e \quad (12)$$

Equation 12 can be linearized as:

$$q_e = \frac{RT}{b}\ln K_T + \frac{RT}{b}\ln C_e \quad (13)$$

Here, RT/b = B (J/mol) is Temkin constant; which is related with the heat of the sorption process; whereas K_T (L/g) reveals the binding constant at equilibrium contact time; R (8.314 J/mol·K) is the universal gas constant; and T° (K) is the absolute solution temperature [42].

Table 8. Model Constants for Langmuir, Freundlich and Temkin equations at different Temperatures

Cation	Temp.(^{0}C)	Langmuir Isotherm				Freundlich Isotherm			Temkin Isotherm		
		q_{max} (mg/g)	K_L (L/mg)	R^2	R_L	K_F (mg/g)(L/mg)$^{1/n}$	$1/n$	R^2	B	K_T (L/mg)	R^2
Cu (II)	30	31.44	0.0037	0.98	0.72	8.56	0.45	0.98	7.51	2.18	0.98
	50	31.74	0.0024	0.88	0.81	10.76	0.42	0.92	5.65	6.42	0.96
	70	31.84	0.0014	0.93	0.88	12.46	0.51	0.97	5.70	8.39	0.99

Freundlich and Temkin model showed higher R^2 values reflecting better linearity for Cu (II) cations at temperature 30, 50 and 70 ^{0}C. The process was favorable as the magnitude for Langmuir separation factor, R_L, and the Freundlich exponent, $1/n$ obtained here was below one. The Langmuir maximum monolayer capacity, q_m was increasing with temperature (Table 8). This observation is consistent with successive increase of Freundlich affinity factor, K_F with the increase of temperature. This reflected that higher temperature had ensured more removal percentage of Cu (II) cations from waste water. Overall it showed the endothermic nature of sorption [16]. This phenomenon was reported earlier for Mn(II) cations sorption onto raw and acid hydrolyzed corncob biomass and mangosteene fruit peel based activated carbon [42, 22].

3.6. Physiochemical Characterization

3.6.1. X-Ray Diffraction (XRD) Analysis

The X-ray diffraction patterns of the raw jute stick powder (JS), hydrochar (JSC) and activated carbon (JSCAC) samples are illustrated by Figure 6. Two narrow, sharp peaks at 2θ values of around 16 and 22° for the raw biomass (JS) were observed due to presence of crystalline cellulose in the sample [43]. For hydrochar (JSC), the intensities of these two peaks were decreased slightly, demonstrating partial cellulose degradation [44]. The XRD pattern of JSC reflected that hydrothermal carbonization could not disrupt the crystalline

texture of cellulose completely. Similar phenomenon was observed for sawdust, wheat straw and corn stalk based hydrochar and KOH treated hydrochar by previous researchers [45]. However, the crystalline cellulose was almost destroyed after activation at higher temperature. Higher pyrolysis temperatures yielded a broader peak at 2θ values of around 22 to 24° in JSCAC sample. This indicated the development of atomic order in the activated sample at higher temperatures [44]. The absence of sharp peaks demonstrated the amorphous texture of the carbon sample [46]. This was expected as amorphous phase materials show better performance as adsorbent due to their high surface area and more active sites over the surface [47]. Previous findings also showed presence of amorphous carbon in coconut coir based activated carbon [48].

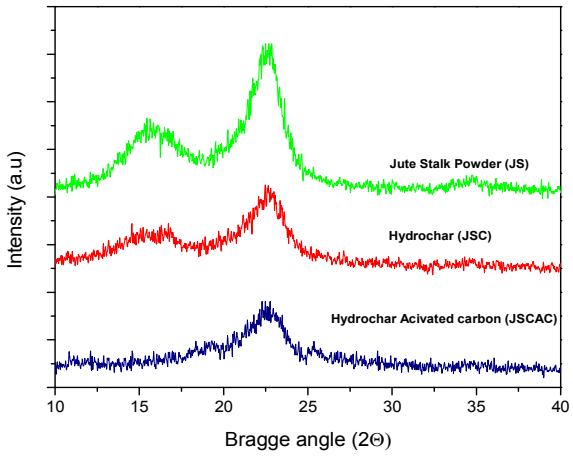

Figure 6: X-ray Diffractograms of (a) Jute stick Powder (JS), (b) Hydrochar (JSC) (c) Hydrochar Activated carbon (JSCAC)

3.6.2. SEM images Analysis

The hydrochar obtained after carbonization was brown in color which represents partially carbonized product. SEM images of raw JS powder, JSC and JSCAC are shown by following Figures of 7a, b and c respectively. The images revealed interesting changes after hydrothermal carbonization (Fig. 7b). SEM image of raw biomass (JS) showed comparatively rough, nonporous texture with some cracks and crevices (Fig. 7a). In contrast to that, SEM images obtained after carbonization (Fig. 7b) reveal substantial changes in surface morphology and texture. Lot of sphere like micro particles was deposited over the larger particles. This indicates that cellulose and hemicellulose were somewhat degraded during hydrothermal carbonization. Thus some microspheres of carbon were found to form [49]. However, non-saccharide component of biomass i.e. lignin is chemically stable than the carbohydrate fraction (Cellulose and hemicellulose). It was partially degraded and the original skeleton of the particles were preserved [9, 14]. After activation, some conchoidal cavities with irregular shaped pores were observed over the surface of JSCAC (Fig.7c). The results demonstrated that a drastic morphological change had taken place due to KOH activation process in presence of CO_2 gas. Similar observation was reported for activation of

eucalyptus wood based hydrochar [45]. The pore structure was clearly visible after activation which means that KOH impregnation and CO_2 gas flow had sweep away the unwanted impurities blocking the pores (Fig.7c) [45]. Consequently pore volume with surface area was extensively increased after the activation process. This was further supported by BET analysis of JSC and JSCAC samples.

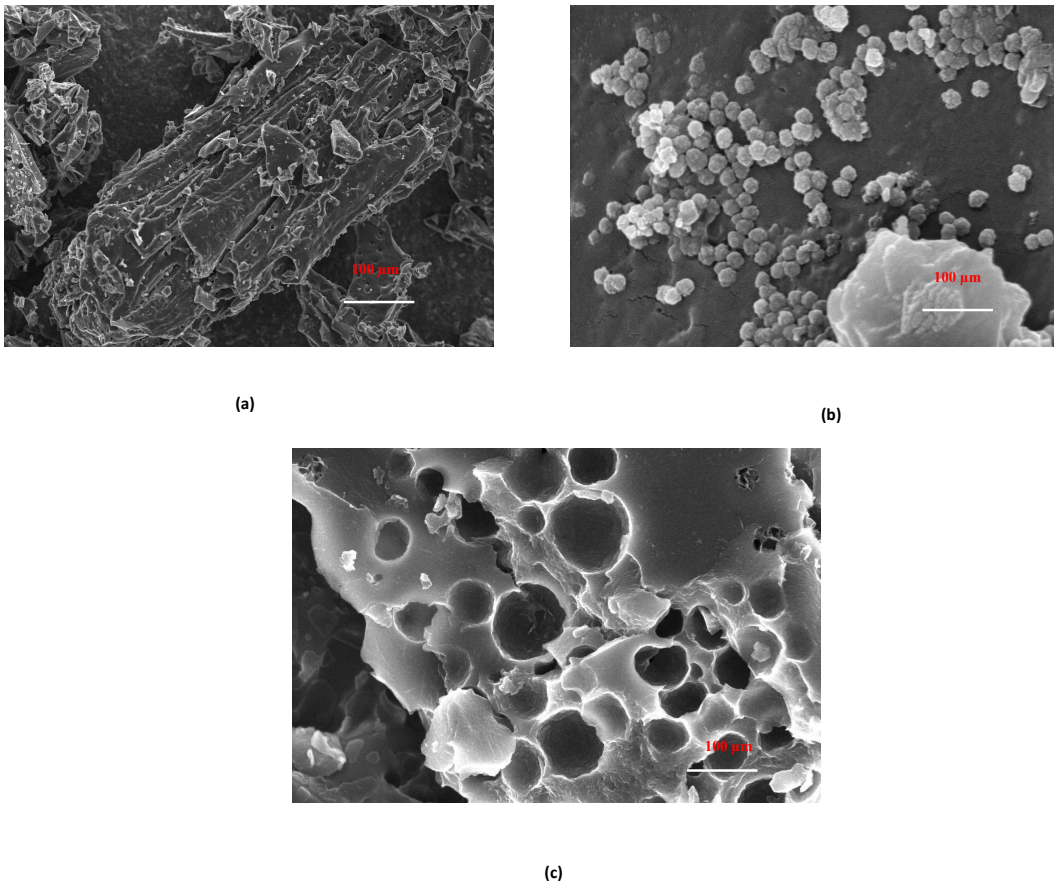

Figure 7: SEM Images of (a) Jute stick Powder (JS), (b) Hydrochar (JSC) (c) Hydrochar Activated carbon (JSCAC)

3.6.3. BET Surface area Analysis

Figure 8a and 8b display the N_2 adsorption isotherms for hydrochar (JSC) and activated hydrochar using KOH (JSCAC) while the textural parameters as determined from these isotherms are listed in Table 9.

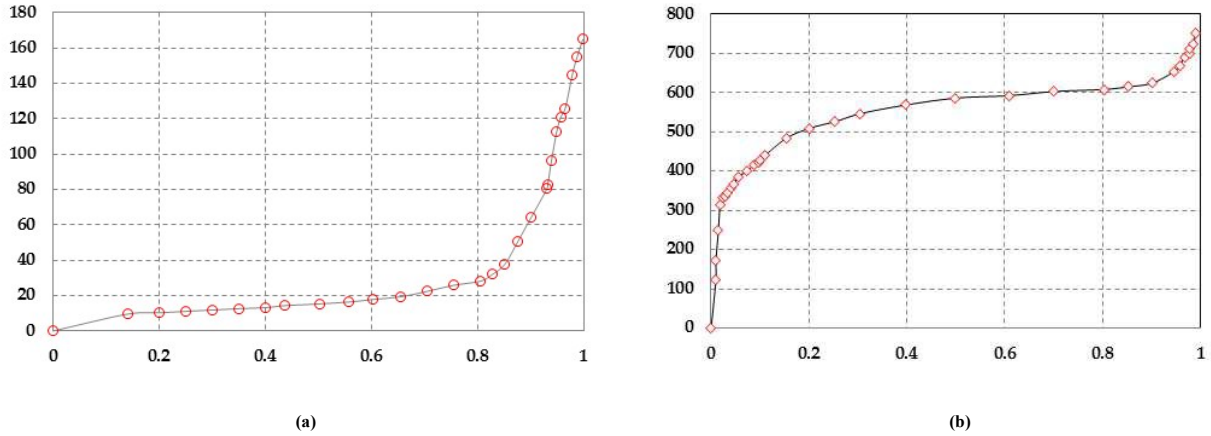

Figure 8: Nitrogen Adsorption Isotherms of (a) Hydrochar (JSC) (b) Hydrochar Activated carbon (JSCAC)

According to IUPAC classification, the isotherm obtained for hydrochar (JSC) can be classified as intermediate between type I and type II isotherm. This indicates a combination of microporous-mesoporous structure with less surface area [10]. After activation in presence of KOH and CO_2 gas, the pore volume increased drastically with enhanced surface area 856.89 m^2/g. The knee of the isotherm obtained for JSCAC appeared more round at low pressure which is usually associated with wide microporous texture [49]. Around relative pressure of about 0.9, the curve showed upward trend. The amount of N_2 gas adsorption was increased with increasing pressure. The shape of the curve indicated a Type II isotherm (Fig. 8b). This indicated the presence of micropores with certain volume of mesopores in JSCAC [25]. The values displayed by Table 9 showed increase of porosity and specific surface area of activated sample (JSCAC) compared to the hydrochar sample (JSC). Due to incomplete carbonization during HTC process, the pores were partially blocked by decomposition products. Activation brings selective removal of those components. In presence of CO_2 gas flow, KOH might react with these structural components over the surface of JSC and induced further depolymerization to increase the pore volume.

Table 9: Pore characteristics of Hydrochar (JSC) and hydrochar activated carbon (JSCAC)

Sample	Specific Surface Area (m^2/g)				Pore Volume (cm^3/g)			Pore Diameter	V_{micro}/V_{Total}
	S_{BET}	S_{Micro}	S_{Meso}	S_{ext}	V_{Total}	V_{Micro}	V_{Meso}	(nm)	%
JSC	3.789	2.709	1.08	2.345	0.256	0.208	0.048	1.304	0.813
JSCAC	856.89	698.76	158.13	559.98	0.889	0.689	0.200	5.896	0.775

The surface area (S_{BET}) of the hydrochar sample enhanced significantly after activation. Due to activation in presence of high temperature, KOH took part in enlargement the pore size and the pore diameter became 5.896 nm for the activated sample (JSCAC). Synergistic effect of temperature, time KOH ratio with CO_2 gas flow had removed the unsaturated carbon atoms and gasified the micro-pore walls to produce more meso-pores [50].

3.6.4. Thermogravimetric (TGA/DTG) Analysis

The thermal stability of (JS), hydrochar (JSC) and activated hydrochar (JSCAC) was investigated using the Thermogravimetric method. The thermal degradation curve for all the samples shows several stages. The first degradation step at approximately 70 to 130° C corresponds to the evaporation of adsorbed water. The second degradation step for JS proceeds in the temperature range of 200 to 300 °C for hemicellulose and 300 to 400 °C for cellulose degradation respectively.

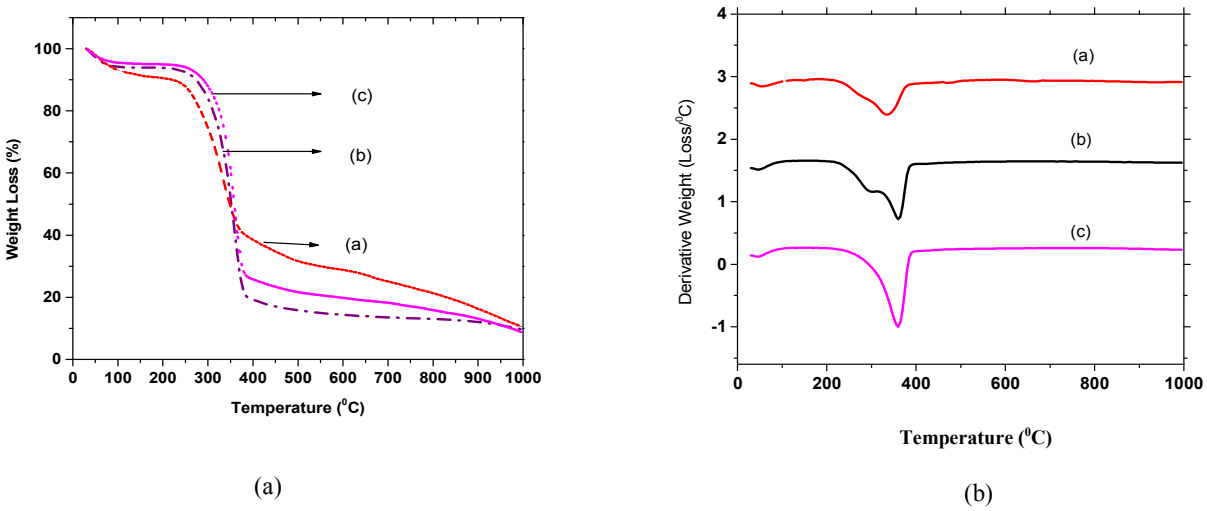

(a) (b)

Figure 9: (a) TGA and (b) DTG Profile of (a) Jute stalk powder (JS) (b) Hydrochar (JSC) (c) Hydrochar Activated carbon (JSCAC)

It was reported earlier that, the degradation of hemicelluloses partially overlaps with cellulose degradation in case of biomass and lignin degradation proceeds within the temperature range of 200 to 800 °C [51]. Compared to JS, JSC and JSCAC showed higher thermal stability. As illustrated by Figure 9, DTG_{max} of JS, JSC and JSCAC were at 346 °C, 356 °C and 360 °C, respectively. Among the three major constituents in lignocellulosic residues, the thermal stability of hemicelluloses was the lowest [52]. Hydrothermal carbonization (HTC) removed hemicelluloses and the amorphous region of the cellulose from JS, leading to an increase of thermal stability in JSC sample. After activation, the sample (JSCAC) contains larger proportion of stable form of carbon particles which is more heat resistant. This phenomenon is evident from elemental analysis also where the percentage carbon in JS was initially 39.81% but after successive treatment of HTC process and activation, it became 87.04%.

3.6.5. Ultimate Analysis

Table 10 lists the ultimate analysis of biomass (JS), hydrochar (JSC) and hydrochar activated carbon (JSCAC). After hydrothermal carbonization, carbon content inside the char matrix was increased, whereas hydrogen and oxygen content was decreased [52]. It can be seen that both H/C and O/C ratio decreased after carbonization and activation [52, 53]. The H/C ratio decreases due to aromatization process during hydrothermal carbonization. O/C ratio decreases for decarboxylation reaction during the process whereas both H/C and O/C ratios decrease due to dehydration reaction [54].

Table 10: Ultimate Analysis of JS, JSC and JSCAC

Ultimate Analysis	JS	JSC	JSCAC
Percentage Carbon	39.81	51.55	87.04
Percentage Hydrogen	6.99	4.56	1.51
Percentage Nitrogen	1.61	1.57	0.80
Percentage Oxygen	49.00	39.56	8.91
Others	2.59	2.76	1.74
H/C	0.175	0.088	0.017
O/C	1.23	0.767	0.102

4. Conclusions

This study explored the potential of utilizing dried jute stalk (JS) based hydrochar (JSC) to prepare activated carbon. The prepared carbon sample (JSCAC) was used to eliminate Cu (II) cations from waste water. Activation conditions for the hydrochar were optimized. Preparation factors were optimized using response surface methodology (RSM) based on Box Behnken Design (BBD). Activation temperature (x_1), time (x_2), ratio (x_3) and CO_2 flow rate (x_4) had substantial influence on each response of removal efficiency as well as production yield. Model validation was done under optimum conditions. It was perceived that the proposed models for Cu (II) removal (Y_1) and yield percentages (Y_2) were significant. The deviation errors obtained between predicted and experimental results for both the models were around 1.30% and 0.348%, respectively. The activated carbon was amorphous with meso-porous texture. After activation, the carbon had surface area of 856.89 m^2/g. The fixed carbon content in the resultant carbon increased substantially up to 87.04 %. The equilibrium data were followed by linear regression analysis at different temperature using Langmuir, Freundlich and Temkin Isotherm showing maximum monolayer sorption capacity about 31.44 mg/g for Cu (II) cations. Better fitting of Freundlich model showed heterogeneous surface with multilayer formation characteristics of Cu(II) cations onto JSCAC. The increasing trend of Langmuir monolayer adsorption capacity with Freundlich affinity factor with temperature clearly revealed that the adsorption process was endothermic in nature. The statistical design methodology used for this research provides a feasible and competent approach for Cu (II) cations removal while minimizing the number of experiment.

Acknowledgments:

The authors would like to thank BKP (BK054-2015) and HIR grant (H-21001-F0032) of University Malaya, Malaysia and Korea Research Foundation, Korea (Research project number: 2013-218-017) for their cordial support in completing this work.

Conflicts of Interest: "The authors declare no conflict of interest."

References

1. Hu B.; Wang K.; Wu L.H.; Yu S.H.; Antonietti M.; Titirici M.M. Engineering carbon materials from the hydrothermal carbonization process of biomass. *Adv. Mater*. **2010,** 22, 813–828.

2. Chowdhury Z. Z., Julkapli N. M., Ali Atieh M., Abdul Rahman AlSaadi M.A.H. , Wageeh A. Y. Microwave Assisted Synthesis, Characterization and Application of Graphitic Bio-carbon using Two Level Factorial Designs, *BioResources*, 2016, 11(2), 3637-3659.

3. Hu B.; Yu S.H.; Wang K.; Liu L.; Xu X.W.; Functional carbonaceous materials from hydrothermal carbonization of biomass: an effective chemical process. Dalton Trans. 2008, 40, 5414–5423.

4. Chowdhury Z.Z., Karim Md. Z., Ashraf M. A. Influence of Carbonization Temperature on Physicochemical Properties of Biochar derived from Slow Pyrolysis of Durian wood sawdust (Durio zibethinus), *BioResources*, 2016, 11(2), 3356-3372.

5. Sevilla M.; Fuertes A.B. Chemical and structural properties of carbonaceous products obtained by hydrothermal carbonization of saccharides. *Chem. Eur. J.* **2009a,** 15, 4195–4203.

6. Sevilla M.; Fuertes A.B.; The production of carbon materials by hydrothermal carbonization of cellulose. *Carbon* **2009b**, 47, 2281–2289.

7. Titirici M.M.; Thomas A.; Antonietti M. Back in the black: hydrothermal carbonization of plant material as an efficient chemical process to treat the CO_2 problem? *New J. Chem*. **2007a**, 31, 787–789.

8. Titirici M.M.; Thomas A.; Yu S.H.; Muller J.O.; Antonietti M. A direct synthesis of mesoporous carbons with bicontinuous pore morphology from crude plant material by hydrothermal carbonization. *Chem. Mater.* **2007b,** 19, 4205– 4212.

9. Sevilla M.; Fuertes A.B. The production of carbon materials by hydrothermal carbonization of cellulose. *Carbon* **2009b,** 47, 2281–2289.

10. Román S.; Valente Nabais J.M.; Ledesma B.; González J.F.; Laginhas C.; Titirici M.M. Production of low-cost adsorbents with tunable surface chemistry by conjunction of hydrothermal carbonization and activation processes, *Microporous and Mesoporous Materials* **2013**, 165, 127–133.

11. Xiu S.; Shabazi A.; Shirley V.; Cheng D. Hydrothermal pyrolysis of swine manure to bio-oil: effects of operating parameters on products yield and characterization of bio-oil. *J. Anal. Appl. Pyrolysis,* **2010**, 88, 73–79.

12. Amaya A.; Medero N.; Tancredi N.; H. Silva H; Deiana C. Activated carbon briquettes from biomass materials. *Bioresour. Technol*. **2007**, 98. 1635–1641.

13. Titirici M. M.; Antonietti M.; Baccile N. Hydrothermal carbon from biomass: a comparison of the local structure from poly- to monosaccharides and pentoses/hexoses, *Green Chem*. **2008**, 10, 1204–1212.

14. Falco C.; Sieben J.M.; Brun N.; Sevilla M.; Van der Mauelen T.; Morallon E.; Cazorla-Amoros, D.; Titirici M.M. " Hydrothermal carbons from hemicellulose-derived aqueous hydrolysis products as electrode materials for supercapacitors, *Chem Sus Chem*, **2013,** 6, 374–382.

15. Chowdhury Z. Z., Abd Hamid S. B., Das R., Hasan M. R., Zain S. M., Khalid K., and Uddin, M. N. Preparation of carbonaceous adsorbents from lignocellulosic biomass and their use in removal of contaminants from aqueous solution, *BioResources. 2013,* 8(4), 6523-6555.
16. Chowdhury Z. Z., Zain S. M., Rashid A.K., Islam Md. S. Preparation and characterizations of fibrous activated carbon from Kenaf for equilibrium adsorption studies of copper from waste water, *Korean Journal of Chemical Engineering*, 2012, 29(9): 1187-1195.
17. Abd. Hamid S.B., Chowdhury Z. Z., Karim Md. Z. Catalytic Extraction of Microcrystalline Cellulose (MCC) from Elaeis guineensis using Central Composite Design (CCD). *BioResources*, 2014, 9(4), 7403-7426.
18. Baskan M.B.; Pala, A. A statistical experiment design approach for arsenic removal by coagulation process using aluminum sulfate", *Desalination*, **2010**, 254, 42–48.
19. Fernandez M.E.; Ledesma B.; Román S.; Bonelli P.R.; Cukierman A.L. Development and characterization of activated hydrochars from orange peels as potential adsorbents for emerging organic contaminants" *Bioresour Technol*, **2015**, 183, 221–228.
20. Chowdhury Z. Z.; Hasan Md.; Abd Hamid S.B.; Shamsudin E.M.; Zain S. M.; Khalid K. Catalytic Pretreatment of Biochar residues derived from Lignocellulosic Feedstock for Equilibrium Studies of Manganese, Mn (II) cations from aqueous solution. *RSC Advances***, 2015**, 5 (9)**,** 6345-6356.
21. Chowdhury Z. Z., Zain S. M., Rashid A.K., and Khalid K. Batch and Fixed bed Adsorption Studies of Lead (II) cations from aqueous solutions onto granular activated carbon derived from *Mangostana garcinia* shell, *Bioresourses*, 2012, 7(3), 2895-2915.
22. Gunaraj V.; Murugan N. Application of response surface methodologies for predicting Weld base quality in submerged arc welding of pipes", *J Mater Process Technol,***1999,** 88, 266–275.
23. Marcos J.C.; Fonseca L.P.; Ramalho M.T.; Cabral J.M.S. Application of surface response analysis to the optimization of penicilin acylase purification in aqueous two-phase system. *Enzyme Microb. Technol*. **2002**, 31, 1006–1014.
24. Karacan F.; Ozden U.; Karacan S. Optimization of manufacturing conditions for activated carbon from Turkish by chemical activation using response surface methodology. *Appl. Therm. Eng*. **2007**, 27, 1212–1218.
25. Karim Md. Z., Chowdhury Z. Z., Abd Hamid S. B. and Ali M. E., Optimizing the pretreatment condition for α-cellulose using lewis acid catalyst, *Science of Advanced Materials*, 2016, 8(3), 534-544.
26. Chowdhury Z. Z.; Zain S. M.; Rashid A. K.; Khalid K. Process Variables Optimization for Preparation and Characterization of Novel Adsorbent from Lignocellulosic Waste. B*ioresourses*, **2012**, 7(3), 3732-3754.
27. Montgomery D.C. Design and Analysis of Experiments. **2001**, Fifth Ed. John Wiley and Sons Inc, New York. pp. 427–500.
28. Sudaryanto Y.; Hartono S. B.; Irawaty W.; Hindarso H.; Ismadji S. High surface area

activated carbon prepared from cassava peel by chemical activation,"*Bioresour. Technol*. **2006,** 97, 734-739.
29. Cao Q.; Xie K. C.; Lv Y. K.; Bao W. R.. Process effects on activated carbon with large specific surface area from corn cob. *Bioresour. Technol.,* **2006**, 97, 110-115.
30. Arenas E.; Chejne F. The effect of the activating agent and temperature on the porosity development of physically activated coal chars. *Carbon* **2004**, 42, 2451–2455.
31. Zolin A.; Jensen A.; Dam-Johansen K.; Jensen L.S. Influence of experimental protocol on activation energy in char gasification: the effect of thermal annealing. *Fuel*, **2001**, 80, 1029–1032.
32. Gratuito M.K.B.; Panyathanmaporn T.; Chumnanklang R.-A.; Sirinuntawittaya, N.; Dutta A. Production of activated carbon from coconut shell: optimization using response surface methodology. *Bioresour. Technol*. **2008**, 99, 4887–4895.
33. Zahangir M. A.; Suleyman A. M.; Noraini K. Production of activated carbon from oil palm empty fruit bunches for removal of zinc," Twelfth International Water Technology Conference, (IWTC12), **2008,** Alexandria, Egypt. pp. 373-383.
34. Suhas Carrott P.J.M.; Ribeiro Carrott M.M.L. Lignin – from natural adsorbent to activated carbon: a review. *Bioresour. Technol*. **2007**, 98, 2301–2312.
35. Bansal R.C.; Donnet J.-B.; Stoeckli F. Active Carbon. **1998,** Marcel Dekker, Inc., New York. p. 482.
36. Lua A.C.; Lau F.Y.; Guo J. Influence of pyrolysis conditions on pore development of oil-palm-shell activated carbons. *J. Anal. Appl. Pyrol*. **2006**, 76, 96–102.
37. Muhlen H.; Van Heek K.H. In: Patrick, W., Jr (Ed.), Porosity in Carbons: Characterization and Applications. **1995,** Halstead Press, London, p. 230.
38. Lua A.C.; Guo J. Activated carbon prepared from oil palm stone by one-step CO_2 activation for gaseous pollutant removal. *Carbon* **2000**, 38, 1089–1097.
39. Langmuir I. The adsorption of gases on plane surfaces of glass, mica and platinum. *J. Am. Chem. Soc.* **1918**, 40, 1361–1403.
40. Chowdhury Z. Z.; Abd Hamid S.B.; Zain S. M. Base Catalytic Approach: A Promising Technique for Activation of Bio Char for Equilibrium Sorption Studies of Copper, Cu (II) ions in Single Solute System. *Materials*, **2014**, *7*, 2815-2832.
41. Freundlich H.M.F. Over the adsorption in solution. *J. Phys. Chem.* **1906***,* 57, 385–471.
40. Temkin M.J.; Pyzhev V. Recent modification to Langmuir isotherms. *Acta Physicochem*, URSS, **1940**, 12, 217–225.
42. Abideen I.A.; Ofudje A.E.; Mopelola A.I.; Sarafadeen O.K. Equilibrium kinetics and thermodynamics studies of the biosorption of Mn(II) ions from aqueous solution by raw and acid treated corn cob biomass. *Am. J. Appl. Sci.* **2011**, 6, 302–309.
43. Yang T.; Lua A. C.Textural and chemical properties of zinc chloride activated carbons prepared from pistachio-nut shells. *Mater. Chem. Phys.* **2006,** 100, 438-444.
44. Keiluweit M.; Nico P. S.; Johnson M. G.; Kleber M. Dynamic molecular structure of plant biomass-derived black carbon (biochar). *Environ. Sci. Technol*. **2010**, 44(4), 1247-1253.

45. Sun K.; Tang J.; Yanyan G.; Zhang H.Characterization of potassium hydroxide (KOH) modified hydrochars from different feedstocks for enhanced removal of heavy metals from water. *Environ Sci Pollut Res***, 2015,** DOI 10.1007/s11356-015-4849-0.
46. Tongpoothorn W.; Sriuttha M.; Homchan P.; Chanthai S.; Ruangviriyachai C. Preparation of activated carbon derived from *Jatropha curcas* fruit shell by simple thermo-chemical activation and characterization of their physico-chemical properties. *Chem. Eng. Res. Des*. **2011**, 8(9), 335-340. DOI: 10.1016/j.cherd.2010.06.012.
47. Tchomgui-Kamga E.; Alonzo V.; Nanseu-Njiki C. P.; Audebrand N.; Ngameni E.; Darchen A. Preparation and characterization of charcoals that contain dispersed aluminum oxide as adsorbents for removal of fluoride from drinking water. *Carbon,* **2010***,* 48, 333–343.
48. Sharma Y.; Gode F. Engineering data for optimization of preparation of activated carbon from an economically viable material. *J Chem Eng Data,* **2010**, 55, 3991-3994.
49. Liu W.; Zhao G. Effect of temperature and time on microstructure and surface functional groups of activated carbon fibers prepared from liquefied wood. *Bioresources*, **2012**, 7(4), 5552-5567.
50. Ishii C.; Suzuki T.; Shino N.; Kaneko K. Structural characterization of heat treated activated carbon fibers. *J Porous Mater*, **1997**, 4(3), 181-186.
51. Gronli M. G.; Varhegyi G.; Diblasi C. (2002). "Thermogravimetric analysis and devolatilization kinetics of wood," *Ind. Eng. Chem. Res*. 41(17), 4201-4208.
52. Zhang Y.; Yang S.; Jian-Quan W.;, Tong-Qi Y.; Sun R. Preparation and Characterization of Lignocellulosic Oil Sorbent by Hydrothermal Treatment of *Populus* Fiber, *Materials* 2014, *7*, 6733-6747.
53. Saqib N.U.; Oh M.; Jo W.; Park S.; Lee J. Conversion of dry leaves into hydrochar through hydrothermal carbonization (HTC). *J Mater Cycles Waste Manag*, **2015**, Doi: 10.1007/s10163-015-0371-1.
54. Liu, F. and Guo, M. (2015). "Comparison of the characteristics of hydrothermal carbons derived from holocellulose and crude biomass" *J Mater Sci*, 50, 1624–1631.